Perceptual Spatial Uniformity Assessment of Projection Displays with a Calibrated Camera

Ping Zhao, Marius Pedersen, Jean-Baptiste Thomas*, and Jon Yngve Hardeberg; Gjøvik University College, Gjøvik, Norway; *Université de Bourgogne, Dijon, France.

Abstract

Spatial uniformity is one of the most important image quality attributes in visual experience of displays. In conventional researches, spatial uniformity was mostly measured with a radiometer and its quality was assessed with non-reference image quality metrics. Cameras are cheaper than radiometers and they can provide accurate relative measurements if they are carefully calibrated. In this paper, we propose and implement a work-flow to use a calibrated camera as a relative acquisition device of intensity to measure the spatial uniformity of projection displays. The camera intensity transfer functions for every projected pixels are recovered, so we can produce multiple levels of linearized non-uniformity on the screen in the purpose of image quality assessment. The experiment results suggest that our work-flow works well. Besides, none of the frequently referred uniformity metrics correlate well with the perceptual results for all types of test images. The spatial non-uniformity is largely masked by the high frequency components in the displayed image content, and we should simulate the human visual system to ignore the non-uniformity that cannot be discriminated by human observers. The simulation can be implemented using models based on contrast sensitivity functions, contrast masking, etc.

Introduction

In the past decade, tremendous growth in the use of digital media implies that our daily life and work have been greatly impacted by the rapid advancement of display technologies. Hence, the image quality assessment of displays become an essential topic for both scientific research and industrial communities. Projection displays have advantages like high resolution, portability and flexibility. For example, multiple projectors can be tiled up to form a large perceptual photometric seamless image [1]. It is cost effective for users to visualize information in a very high resolution without issuing a customized manufacturing demand.

In general, the image quality of displays can be characterized by groups of image quality attributes. One group of them includes physical screen dimension, display resolution, refreshing rate, viewing distance, and viewing angle etc. These attributes are associated with a specific display and its viewing condition. They indeed have impacts on the perceptual image quality, but in most cases they are assumed to be constants within one working cycle of image quality assessment. The rest of the attributes include, but are not limited to, brightness, contrast, color gamut, sharpness and artifacts (including noises). Among these attributes, the spatial uniformity can be of a major importance for projection displays [2, 3]. Researchers tried to achieve objective spatial uniformity with mathematical modeling, but soon they realized that some restraints can be relaxed due to the limitation of perception of Human Visual System (HVS) [1]. In recent studies [4, 5, 6], radiometers were used as absolute acquisition devices to measure the luminance and chrominance of projection displays. Measuring with radiometers is time consuming. The devices are expensive and they are likely to be unavailable in real practice. Digital still cameras have been used to record projection pixels including its background and surrounding on the displays [7, 8, 9]. Cameras have the advantage that they can be placed at different locations in order to achieve a location- and view-dependent image quality assessment, and the acquisition process are much accelerated. However, cameras offer relative sensor responses upon the incoming lights, so they need to be carefully calibrated in advance.

In this paper, we propose and implement a work-flow to use a calibrated camera as a relative acquisition device to record the intensity of projections, and evaluate the spatial uniformity of projections against image quality metrics. The correlation between perceived and measured results suggest that the camera based image quality assessment can be reliable and accurate.

This paper is organized as follows: first, in the background section, we review the existing image quality metrics for spatial uniformity assessment. Then in uniformity assessment section, we describe the setup of our control lab environment, and demonstrate how to calibrate a camera and a projector to produce multiple levels of linearized non-uniformity on the projection screen. In addition, we also describe the experiment procedure and show the experiment results. In the last section, the conclusions and future works are presented.

Background

Many uniformity metrics have been proposed based on luminance measurements of gray patches. Among the international standards for image quality assessment of displays, FPDM [10] defines uniformity as $(100\% \cdot (L_{min}/L_{max}))$, where L_{min} and L_{max} stand for minimum and maximum measured luminance respectively. TCO 6.0 [11] defines a compliance threshold based on four luminance samples as (L_{max}/L_{min}), assuming that the minimum luminance is not even close to zero. SPWG [12] defines uniformity as $(100\% \cdot (L_{max} - L_{min})/L_{max})$ based on thirteen independent luminance measurements. These metrics associate uniformity with Luminance Ratio (LR) between two extreme pixels.

However, Tang [13] and Ngai [14] demonstrated that the LR based methods have inaccurate predictions of the non-linear HVS. Tang [13] incorporated the viewing distance d and spatial derivatives s of luminance to define the uniformity as $SFA = d^2\left(L_{max} + L_{min} - 2\overline{L}\right)/s^2$, where $\overline{L}$ stands for the average of measured luminance. Further research from Samuelson et al. [21] quantify the image quality of an illuminated surface with a proposed spatial frequency analysis algorithm incorporating the dif-

ference of Gaussian function, and they suggested that the average magnitudes of luminance contrast within selected spatial frequency bands are related to the lighting quality of the scene represented by the image. Beyond these studies, Ashdown [15] investigated the influence of Luminance Gradient (LG) on the spatial uniformity and they indicated that their results were more correlated to the subjective perceptual ratings than LRs. However, these studies ignore the factor of viewing distance which is important to the uniformity assessment. Meanwhile, other metrics based on statistical analysis and/or color distances in specific color spaces were proposed. Poulin et al. [16] proposed a metric to determine the spatial uniformity as $(100\% - STDEV(L))$, where $STDEV(L)$ stands for the standard deviation (STDEV) of luminance. Thomas et al. [4] used color differences ΔL and ΔC measured with a spectroradiometer. The results suggested that the chromaticity shifts are significant and they should be accounted for. Another statistics based uniformity is defined as the variation of coefficient $\sqrt{\sum_{i=1}^{N}(L_i - \overline{L})}/(\overline{L}(N-1))$, where N stands for the number of sample points [17].

There are also existing works that are relevant to the uniformity assessment based on captured images. In the domain of printing, Green [18] proposed a metric for measuring smoothness of color transforms. The metric computes the second derivative from the vector of color differences. Besides, wavelet analysis [19] and standard deviation [20] are common methods to analyze non-uniformity (mottle). These methods were originally designed for printings, but they can be used for displays in a similar fashion.

Uniformity Assessment

In this section, we describe the experimental setup and how to use a camera and a projector to produce multiple levels of non-uniformity on the projection display.

Experimental Setup

The experiments take place in a controlled lab environment where the only illuminant in the room is the projector. We use a portable three chip LCD projector SONY APL-AW15 (throw ratio: 1.5) to produce projections on a planar screen which is naturally hanging on the ceiling. The projector is placed on a table in front of the projection screen, and the distance is approximately 3m with respect to the throw ratio of the projector. A remote controlling laptop is connected to the projector via a VGA cable in order to generate full screen projections which have resolution 1280×768 in pixels. On the screen, the dimension of projection area is approximately 2×1.2 in meters. We use a DLSR Nikon D610 which has an imaging resolution 6048×4016 in pixels and with a Sigma VR 24-105mm f/4G (VR off) lens to capture the projections. The camera is fixed on a tripod and the pictures are taken remotely with a software control on the laptop without physically touching the camera. The pictures are saved in raw format and rendered with Aliasing Minimization and Zipper Elimination demosaicing algorithm [22] without automatic vignette correction, brightness adjustment, gamma correction and noise reduction etc.

Vignetting Correction

Captured pictures are known to have vignetting effect which stands for an undesirable gradual intensity fall off from the image center to its external limits. In this paper, we correct camera vignetting based on the captures of a hazy sky which is closely uniform in gray [23]. In the lab, we take several trial shots of projections with either minimum or maximum projector input intensity. In this process, we adjust the camera settings iteratively until all the captures are neither underexposure nor overexposure. Then we keep all camera settings except exposure time, hook a neutral light diffuser (white and semi-transparent) over the camera lens, and use the camera to take multiple pictures toward the same spot of the hazy sky. Each time we take a picture we rotate the camera a bit. Then we calculate the intensity median response for each camera pixel over all pictures we have taken, and use them to generate a vignetting mask which is then applied to the camera RGB channels separately to correct the vignetting.

In the experiment, we take 60 pictures of the hazy sky and put 40 of them into a training set and the rest into a validation set. The median responses are obtained based on 5, 10, ..., and 60 pictures in the training set respectively. Then we apply corresponding masks to the pictures in the validation set. The minimum averaged standard deviation over all validation pictures indicate that empirically 10 pictures are sufficient to generate convergent median results. The mask we generate for our camera is shown in Figure 2. We can see that the vignetting is not even closely symmetric. The center has shifted upward and also a bit to the right. This observation is contrary to common assumptions about the vignetting symmetry in many literature (cos four law [24] for example). In order to maximize the validity and reliability of image quality assessment, we should offer the best effort to avoid assumptions. Our method places no assumption about the camera or the light condition, and the whole procedure can be finished within a few minutes.

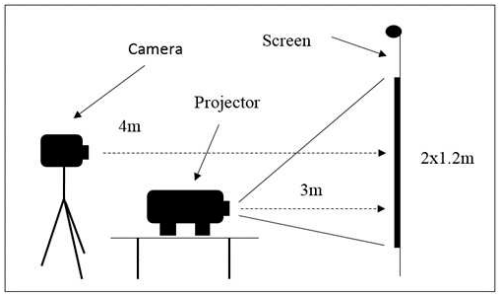

Figure 1. *Experiment setup (throw ratio: 1.5)*

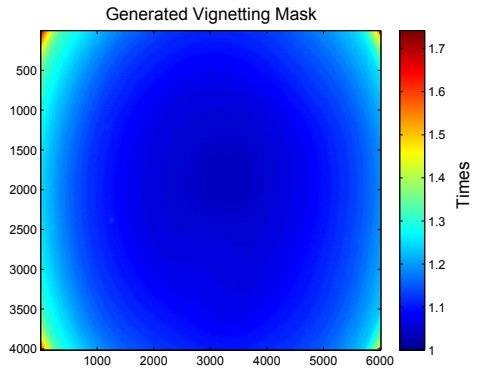

Figure 2. *The generated vignetting mask for our camera Nikon D610 with a Sigma VR 24-105mm f/4G (VR off) lens*

Exposure Optimization

The daylight environment has a much higher luminance (normally above 1000 Lux) than the projection environment (around 10 Lux for example). In order to avoid either underexposure or overexposure of captures, the camera's exposure time varies between the two light conditions. The vignetting mask generated in a daylight condition might not be appropriate for the low light condition, since in this context we implicitly assume that all camera sensors have linear responses. In order to verify the linearity, we equally separate the range of projector input intensity into 15 levels. For each level, we display a gray patch and capture it under all possible camera exposure times ranging from 1/4000s to 30s. Meanwhile, we use a light meter to measure the physical luminance on the projection screen as a reference to the camera. Then we construct surfaces of camera intensity responses versus the projector luminance and camera's exposure time.

The first picture in Figure 3 depicts the intensity response of one camera sensor in the red channel. In the deep blue region, the responses are closely linear to all possible projector luminance while the exposure time is fixed, and vice versa. However, in the aqua regions, such sensor has a large boost in responses. It may be argued that this is because the camera sensor is closely saturated in these cases. Then we can have a look at the second picture in Figure 3 where the responses of another camera sensor in the green channel is obviously not saturated. In this case, the boost is still available at the areas where the blue and aqua regions intersect. In this context, we can see that the camera gives linear responses corresponding to limited combinations of projector luminance and camera's exposure time.

This conclusion seems to be trivial because the exposure time should be kept below 2s in most cases. However, in order to apply the vignetting mask generated in a high light condition to a low light condition, we have to make sure that the camera responses are all linear with respect to a common exposure time. For this reason, we determine the strongest responses over each camera intensity response for the maximum luminance under the two light conditions with a common exposure time, and we continue to decrease the exposure time until the ratios between such two sensor responses are equal. However, applying an exposure time which is too small would not take the full advantage of the dynamic range of the camera. Once this condition is met, the camera's exposure time is optimized, and the generated vignetting mask can be applied to the camera despite of light conditions.

Image Registration

In the context of image quality assessment incorporating full reference metrics, it is critical to achieve accurate and automatic image registration between the captured image and its reference image. Then we can apply existing full reference metrics with no modification to them. The preservation of geometrical order as well as the color relationships between two consecutive pixels on displays are maximized. In our previous research [25], we proposed a marker-less and view-independent method to use a camera to do the image registration. The maximum pixel shift error is below 0.2 pixel in the cases that camera resolution is higher than projection resolution. With respect to the performance evaluations with SSIM metric [28], the image registration accuracy is higher than 0.95 in a dark room environment and it is above 0.9 in a dimmed light condition where ambient light is below 30

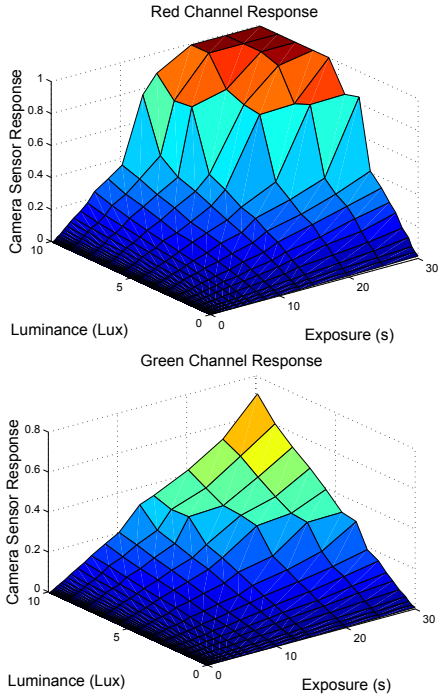

Figure 3. *Intensity responses of one camera sensor in the red channel (1st picture), and another sensor in the green channel (2nd picture)*

Lux. In this paper, we adopt this method to extract projections from the captured images, and make them have exactly the same dimension and resolution as their reference images.

Projector Calibration

In order to assess the perceptual spatial uniformity, we produce multiple levels of linearized non-uniformity on the screen to be observed and captured. Brown et al. [9] located the minimum common achievable projector response for all pixels and generated a luminance attenuation map to correct the projection colors. The linearity of projector's intensity responses is assumed; otherwise the inverse projector intensity transfer function is applied to compensate for that. Pagani et al. [23] proposed a shading table based automatic uniformity correction. The colors of each shading point are corrected by iteratively refining the projector output intensities in order to avoid temporary stability problem of projectors, and the colors of other pixels are linearly interpolated based on its shading point neighbors.

In this research, we adopt and extend the method proposed by Brown et al. [9] for its simplicity and effectiveness. First, we equally separate the range of projector input intensity into 15 levels, and for each level we display and capture a gray patch 10 times. Then the projector intensity transfer functions can be recovered by polynomial regression upon the median responses over the gray patches at all intensity levels. In this way, we can avoid the temporary stability problems of both camera and projector. However, it is computational inefficient to determine the regression coefficients for all twenty million pixels of the camera Nikon D610. We calculate only the coefficients for the reference pixel which gives the lowest camera sensor response upon maximum projector luminance. The coefficients for other pixels can be obtained by linearly scaling the one of the reference pixel.

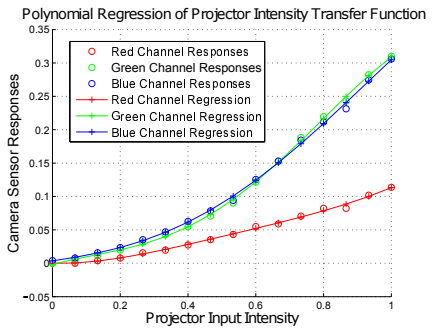

Figure 4. *Polynomial regression of camera sensor responses*

The method is processed in a color channel basis. After this, we inverse the regression functions to compensate the non-linearity of camera responses in order to create flattened projections. In our experiment, 5th order polynomial regression is sufficient to achieve good approximation. The projectors intensity transfer functions for the reference pixel are depicted in Figure 4. Lower order regressions (2nd order for example) produces slightly different curves, but they may cause overcasting of dominated colors. The polynomial regression may produce negative values which are invalid. In such cases, we simply clip them because the absolute values are small $(< 1e-3)$ to be negligible.

Suppose that the scaling ratio of one pixel p_{ij} in an individual color channel on the ith row and jth column of the registered image is $r_{ij} \geq 1$, the corresponding regression function for the reference pixel is $f(x)$ and its inverse function is denoted as $f^{-1}(x)$. The x stands for the projector input intensity of the pixel p_{ij}. The camera response of pixel p_{ij} is denoted as $c_{ij} = f(x) \cdot r_{ij}$. In this context, the projector input intensity for the pixel p_{ij} at a certain non-uniformity level is defined as $g(x) = f^{-1}\left(f(x) \cdot s\left(r_{ij} - m\right)\right)$, where $m = \sum_{i=1}^{n_y} \sum_{j=1}^{n_x} r_{ij} / \left(n_x \cdot n_y\right)$, n_x and n_y stand for the width and height for the projection in pixels respectively, and s stands for a linear scaling factor of non-uniformity and it is under the constraint that $f(0) \cdot r_{ij} \leq g_{ij}(x) \leq f(x) \cdot r_{ij}$ assuming that the projector input intensities are normalized to between 0 and 1. The value of r_{ij} can be determined as $max\left(c_{ij}\right) / f(1)$, where the operator max stands for the maximum value of c_{ij}.

Experimental Procedure

We incorporate human observers and full reference image quality metrics to assess the spatial uniformity of projection displays. We display seven types of test images (see Figure 5): two natural color pictures (the 15th and 23th picture from Kodak Photo CD PCD0992 [26]), three uniform colored patches with opponent colors: yellow, magenta and cyan respectively, one gray patch (the gray level equals to 0.5) and one slide like image with dark texts on a gradient background. For each test image, we linearly scale its natural projection's non-uniformity to produce multiple levels of non-uniformity. These scaling ratios can be normalized into the range between -1 and 1, and then we split it into five levels: -0.6, -0.2, 0, 0.2 and 0.6. The level 0 corresponds to flattened projections where the projector's natural non-uniformity is canceled. We also display one image reserving the projectors natural non-uniformity by displaying the image as it is; so 42 images in total are presented to each human observer.

The viewing condition is similar to a home theater environment where the room is dark, and the observers are located at the camera's position. The test images are displayed to observers in a randomized order. The experiment is set up as a category judgment experiment. So, for each displayed image, the observers are asked to indicate the perceptual uniformity with a category label which stands for the rank between not uniform at all and perfectly uniform corresponding to the ratings numbers from 1 to 5. At the same time, the observers are also asked to indicate how the non-uniformity affect their pleasantness with a category label which stands for the rank between very disturbing and not disturbing at all corresponding to the rating numbers from 1 to 5. The perceptual ratings are collected from 10 human observers and then they are scaled to generate Z-scores [28].

We also evaluate the uniformity with the following image quality metrics: LR defined in VESA FPDM [10], LG based definition [13] (SFA), averaged standard deviation of RGB values (Stddev), coefficients of variation [17] (Coeff), averaged Euclidean distance $\overline{\Delta E^*_{ab}}$ in CIELAB color space (ΔE_{ab}), PSNR-M [27], SSIM [28], and S-CIELAB [29]. The first four metrics are commonly referred uniformity metrics in literature, while the metrics $\overline{\Delta E^*_{ab}}$ is frequently referred to determine the perceptual distance between two colors. Since the non-uniformity changes the structure information in the images, we adopt SSIM as well.

Subjective Results

The first observation is that the rank order of non-uniformity is largely preserved for the seven types of test images as expected (see Figure 5). If we assume that the general tendency of Z-scores are smooth, then they can be represented by parabolic curves. The curves might be more or less skewed depends on the projected image content. The flattened projections do not necessary correspond to the highest overall Z-scores, while small negative non-uniformity and natural projection images have similar or relative lower Z-scores in many cases, and either positive or negative large non-uniformity leads to the lowest Z-scores. This observation supports the fact that HVS is not sensitive to small variation of non-uniformity. The spatial non-uniformity is largely masked by the high frequency components in the displayed image content, and we should simulate the human visual system to ignore the non-uniformity that cannot be discriminated by human observers. The simulation can be implemented using models based on contrast sensitivity functions, contrast masking, etc. For the distorted slide like images (correspond to the 7th test image), the Z scores of flattened versions are clearly greater than others (higher mean value and no overlapping of confidence intervals). This is because such reference image has dark texts on a large gradient background in a bright color, and the non-uniformity on a gradient background can be easier to be detected by HVS than that on a flat background which is the case of a gray patches (correspond to the 1st test image). The general tendency of mean Z-scores of pleasantness are very similar to the ones of perceived uniformity and the Pearson correlation between them are all above 0.98 for all test images, except the absolute mean values of pleasantness are slightly larger in general. This observation suggests that the HVS has a certain degree of but limited tolerance on average against non-uniformity on the display. For the gray patch test images, the observers have a difficulty to distinguish the differences between the small minus non-uniform, flattened, natural projections. In a similar fashion, the pleasantness of small minus non-uniformity, flattened and natural projections for the two natural images have

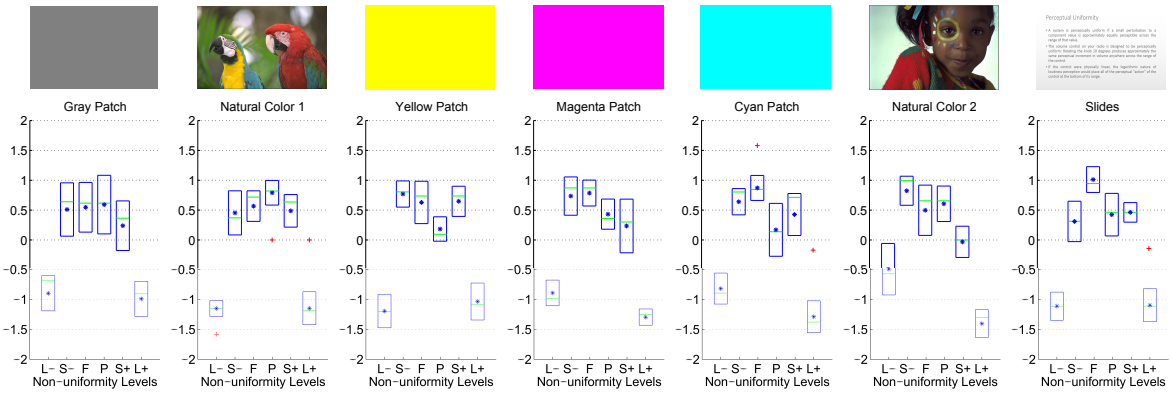

Figure 5. *Mean Z-scores of perceived uniformity, the blue box indicates the 95% confidence interval of Z-scores, the green bars stand for the median values of Z-scores, and the red crosses stand for the outliers with respect to quartile based statistic tests (against outer fences)*

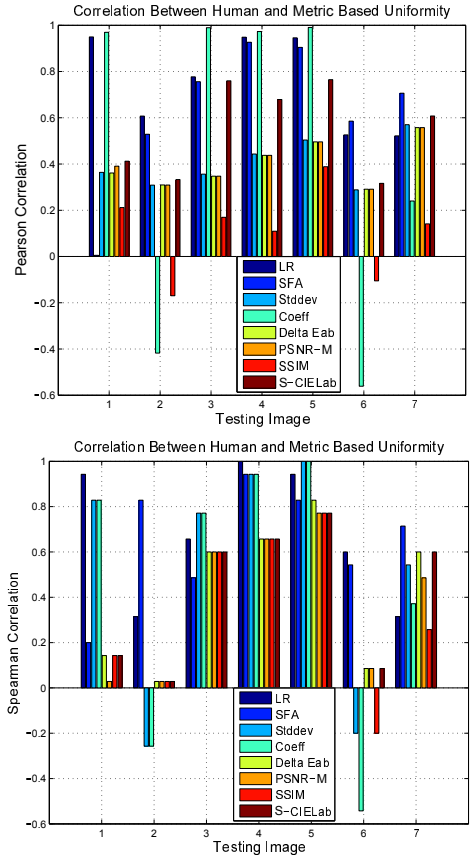

Figure 6. *Pearson (1st picture) and Spearman (2nd picture) correlations between the mean Z-scores of subjective ratings and objective metric results*

similar values but their corresponding perceived uniformity have different mean values. This observation suggests that the non-uniformity is masked by the complex colors of natural pictures and in such cases achieving a restrained uniform is not the only way to produce the best perceptual experience.

Objective Results

Figure 6 demonstrates the Pearson and Spearman correlations between the mean Z scores of perceived uniformity and objective results from all metrics. Obviously, none of these metrics works well for all types of images, especially for natural color images (the 2nd and 6th test images). Simple metrics like LR and SFA work surprisingly better than others in many cases. We think this might because in our experiment the non-uniformity for all pixels is globally scaled, so the rank order of intensities in each primary color channel is largely preserved; although we apply negative scalars to non-uniformity as well, the magnitude of scaled non-uniformity is still comparatively smaller than the reference intensity values in the reference images. However, in real practice, the non-uniformity level of projections should be relatively small, otherwise the optical components of such a projector should be replaced with new ones. The metric Coeff also gives high correlation scores for patches but negative values for natural pictures (the 2nd and 6th test images). However, no metric works well for the natural color images and slide like images (the 7th test images). In such cases, the correlation values are largely below 0.6. S-CIELAB also adopts CSF but it has slightly better correlation results than PSNR-M and SSIM metrics in all cases. It is also interesting to figure out the reason why metric LR does not work well in many cases, so we generate the plots of the subjective results versus the objective results for the LR metric (see Figure 7). It is clear that for the non-patch test images, the variance of metric scores are largely compressed and a few outliers are visible. By examining the metric score values, we find out that these outliers correspond to the flattened projection and natural projection. Similar phenomenon can be observed for other metrics. It suggests that either the metrics give lower values for the flattened projection, or higher values for the natural projection comparing to their expected values. In other words, the distance between the two consecutive levels of perceived uniformity is more compressed than the results of metrics.

Conclusion and Future Works

In this paper, we propose and implement a work-flow to use a calibrated camera as a relative acquisition device of intensity to measure the spatial uniformity of projection displays. The experimental results suggest that none of the frequently referred spatial uniformity metrics works well for all types of test images, especially for the flattened projections and natural projection of natural color images. In such cases, The spatial non-uniformity is largely masked by the high frequency components in the displayed image content, and we should simulate the human visual system to ignore the non-uniformity that cannot be discriminated by human observers. The simulation can be implemented using

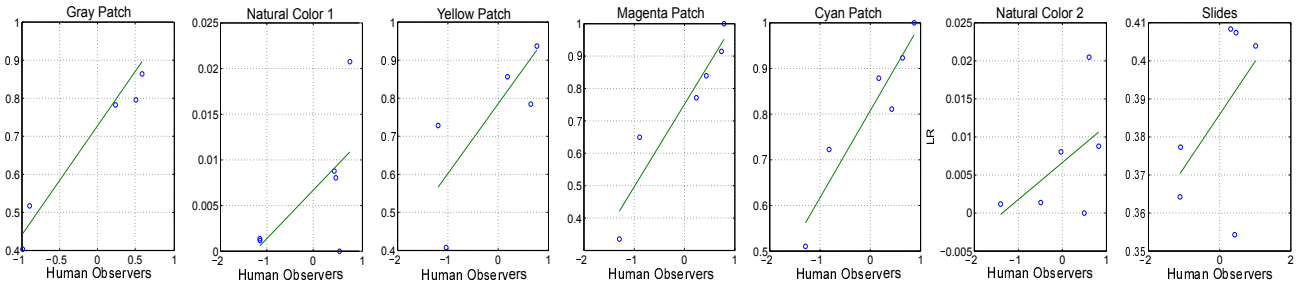

Figure 7. *LR metric scores versus subjective mean Z-scores for all test images*

models based on contrast sensitivity functions, contrast masking, etc. In addition, the colors can be considered to be transformed into the frequency domain and analyzed at a smaller granularity in order to engage the issue of contrast masking. In the coming future, we should either improve the existing metrics or design a new one to evaluate the spatial uniformity of projection displays. Such a metric should be incorporated into a unified image quality assessment framework for projection displays.

References

[1] A. Majumder and R. Stevens, Perceptual Photometric Seamlessness in Projection-based Tiled Displays, ACM Trans. Graph., vol. 24, no. 1, pp. 118-139, Jan. 2005.

[2] A. M. Bakke, J. B. Thomas, and J. Gerhardt, Common Assumptions in Color Characterization of Projectors, in Gjøvik Color Imaging Symposium, 2009, pp. 45-53.

[3] J. Thomas, A. M. Bakke, and J. Gerhardt, Spatial Nonuniformity of Color Features in Projection Displays: A Quantitative Analysis, J. Imaging Sci. Technol., vol. 54, no. 3, p. 030403, 2010.

[4] J. B. Thomas and A. M. Bakke, A Colorimetric Study of Spatial Uniformity in Projection Displays, in Computational Color Imaging, vol. 5646, A. Trémeau, R. Schettini, and S. Tominaga, Eds. Springer Berlin Heidelberg, 2009, pp. 160-169.

[5] G. Menu, L. Peigne, J. Y. Hardeberg, and P. Gouton, Correcting Projection Display Non-uniformity Using A Webcam, in Color Imaging X: Processing, Hardcopy, and Applications, 2005, pp. 364-373.

[6] J. B. Thomas, Colorimetric Characterization of Displays and Multidisplay Systems, Université de Bourgogne, 2009.

[7] R. Raskar, M. S. Brown, R. Yang, W. C. Chen, G. Welch, H. Towles, B. Seales, and H. Fuchs, Multi-projector Displays Using Camera-based Registration, in IEEE Visualization, 1999, pp. 161-168.

[8] R. I. Hartley, Self-Calibration from Multiple Views with a Rotating Camera, in European Conference on Computer Vision, 1994, pp. 471-478.

[9] M. Brown, A. Majumder, and R. Yang, Camera-based Calibration Techniques for Seamless Multiprojector Displays, IEEE Trans. Vis. Comput. Graph., vol. 11, no. 2, pp. 193-206, 2005.

[10] Flat Panel Display Measurements Standard 2.0. Video Electronics Standards Association, Newark, USA, pp. 1-18, 27-Oct-2005.

[11] TCO Certified Displays 6.0. TCO Development AB, Stockholm, Sweden, pp. 1-125, 27-Oct-2012.

[12] SPWG Notebook Panel Specification 3.8. Standard Panel Working Group, Newark, USA, pp. 1-59, 2007.

[13] T. Ling, The Assessment of Ceiling Uniformity for Indirect Lighting Systems, 1996.

[14] P. Y. Ngai, The Relationship Between Luminance Uniformity and Brightness Perception, J. Illum. Eng. Soc., vol. 29, no. 1, pp. 41-50, Jan. 2000.

[15] I. Ashdown, Luminance Gradients: Photometric Analysis and Perceptual Reproduction, J. Illum. Eng. Soc., vol. 25, no. 1, pp. 69-82, Jan. 1996.

[16] F. Poulin and M. Caron, Display Measurement - A Simple Approach to Small-area Luminance Uniformity Testing, Television Displays, pp. 1-9, 2009.

[17] M. S. Rea, Ed., The IESNA Lighting Handbook - Reference and Application, 9th editio. Illuminating Engineering, 2000, pp. 1-1000.

[18] P. J. Green, A Smoothness Metric for Colour Transforms, in Color Imaging XIII: Processing, Hardcopy, and Applications, 2008, vol. 6807, p. 68070I-68070I-5.

[19] J. P. Bernie, H. Pande, and R. Gratton, A New Wavelet-based Instrumental Method for Measuring Print Mottle, Measuring Instruments, vol. 9, pp. 197-199, 2004.

[20] A. Sadovnikov, P. Salmela, L. Lensu, J. K. Kamarainen, and H. Klvinen, Mottling Assessment of Solid Printed Areas and Its Correlation to Perceived Uniformity, in Scandinavian Conference on Image Analysis, 2005, vol. 3540, pp. 409-418.

[21] C. E. Samuelson, I. Ashdown, P. Kan, A. Kotlicki, and L. A. Whitehead, A Proposed Lighting Quality Metric Based on Spatial Frequency Analysis, in Illuminating Engineering Society Annual Conference, 1999, pp. 51-61.

[22] E. Martinec and P. Lee, AMAZE Demosaicing Algorithm, 2010. [Online]. Available: http://www.rawtherapee.com/. [Accessed: 04-May-2014].

[23] A. Pagani and D. Stricker, Spatially Uniform Colors for Projectors and Tiled Displays, J. Soc. Inf. Disp., vol. 15, no. 9, p. 679, 2007.

[24] D. A. Kerr, Derivation of the Cosine Fourth Law for Falloff of Illuminance Across a Camera Image.pp. 1-12, 2007.

[25] P. Zhao, M. Pesersen, J. Y. Hardeberg, and J. B. Thomas, Image Registration for Image Quality Assessment of Projection Displays, in IEEE International Conference on Image Processing, 2014.

[26] R. Franzen, PhotoCD PCD0992, Kodak Lossless True Color Image Suite, 1999. [Online]. Available: http://r0k.us/graphics/kodak/. [Accessed: 11-May-2014].

[27] N. Ponomarenko, F. Silvestri, K. Egiazarian, M. Carli, J. Astola, and V. Lukin, On Between-coefficient Contrast Masking of DCT Basis Functions, in Proceedings of the Third International Workshop on Video Processing and Quality, 2007, pp. 1-4.

[28] Engeldrum, P. G. (2000). Psychometric Scaling: A Toolkit for Imaging Systems Development (pp. 1-200). Imcotek Pr.

[29] Z. Wang, A. C. Bovik, H. R. Sheikh, and E. P. Simoncelli, Image Quality Assessment: from Error Visibility to Structural Similarity, IEEE Trans. Image Process., vol. 13, no. 4, pp. 600-612, Apr. 2004.

[30] G. M. Johnson and M. D. Fairchild, A Top Down Description of S-CIELAB and CIEDE2000, Color Res. Appl., vol. 28, no. 6, pp. 425-435, Dec. 2003.